

# Improving AlN Crystal Quality and Strain Management on Nanopatterned Sapphire Substrates by High-Temperature Annealing for UVC Light-Emitting Diodes

Sylvia Hagedorn,\* Sebastian Walde, Norman Susilo, Carsten Netzel, Nadine Tillner, Ralph-Stephan Unger, Phillip Manley, Eviathar Ziffer, Tim Wernicke, Christiane Becker, Hans-Jürgen Lugauer, Michael Kneissl, and Markus Weyers

Herein, AlN growth by metalorganic vapor-phase epitaxy on hole-type nanopatterned sapphire substrates is investigated. Cracking occurs for an unexpectedly thin-layer thickness, which is associated to altered nucleation conditions caused by the sapphire pattern. To overcome the obstacle of cracking and at the same time to decrease the threading dislocation density by an order of magnitude, high-temperature annealing (HTA) of a 300 nm-thick AlN starting layer is successfully introduced. By this method, 800 nm-thick, fully coalesced and crack-free AlN is grown on 2 in. nanopatterned sapphire wafers. The usability of such templates as basis for UVC light-emitting diodes (LEDs) is furthermore proved by subsequent growth of an UVC-LED heterostructure with single peak emission at 265 nm. Prerequisites for the enhancement of the light extraction efficiency by hole-type nanopatterned sapphire substrates are discussed.

Common UVB- and UVC-LEDs are based on AlGaInN heterostructures. They are typically fabricated as bottom emitters. Therefore, transparent substrates from AlN bulk material would be an ideal base for such devices, but the price of native substrates is still relatively high and large quantities are not yet available. As a compromise, usually AlN grown by metalorganic vapor-phase epitaxy (MOVPE) on sapphire substrates is used. These templates are transparent in the UV spectral range, available at relatively low costs but suffer from threading dislocations that lower the efficiency of LEDs. During the past 15 years, many publications dealt with the topic of threading dislocation density (TDD) reduction in AlN. Among the differ-

## 1. Introduction

Light-emitting diodes (LEDs) emitting in the UVB and UVC spectral range can potentially cover a broad field of applications. They are not only an ecologically friendly and compact alternative to mercury lamps but also open new fields of applications due to easy implementation and the defined wavelength. Many different fields of application for UV-LEDs can be found, for example, phototherapy, UV curing, and water disinfection.<sup>[1–4]</sup>

ent approaches, there are many approaches that use the annihilation of dislocations with increasing layer thickness ( $>3 \mu\text{m}$ ). Therefore, the techniques to overcome the cracking of AlN layers at layer thicknesses above  $1 \mu\text{m}$  were developed mainly based on “rough to smooth” growth approaches<sup>[5,6]</sup> or by substrate patterning and subsequent lateral overgrowth processes.<sup>[7,8]</sup> TDD values reached are about  $5 \times 10^8 \text{ cm}^{-2}$ , but commercially available AlN/sapphire templates still tend to be in the TDD range of  $10^9 \text{ cm}^{-2}$ .<sup>[9–11]</sup> This shows that the development of a stable,

Dr. S. Hagedorn, S. Walde, C. Netzel, R.-S. Unger, M. Kneissl, M. Weyers  
Ferdinand-Braun-Institut  
Leibniz-Institut fuer Hoechstfrequenztechnik  
Gustav-Kirchhoff-Str. 4, 12489 Berlin, Germany  
E-mail: Sylvia.Hagedorn@fbh-berlin.de

N. Susilo, E. Ziffer, T. Wernicke, M. Kneissl  
Institute of Solid State Physics  
Technische Universität Berlin  
Hardenbergstr. 36, 10623 Berlin, Germany

 The ORCID identification number(s) for the author(s) of this article can be found under <https://doi.org/10.1002/pssa.201900796>.

© 2020 The Authors. Published by WILEY-VCH Verlag GmbH & Co. KGaA, Weinheim. This is an open access article under the terms of the Creative Commons Attribution License, which permits use, distribution and reproduction in any medium, provided the original work is properly cited.

DOI: 10.1002/pssa.201900796

N. Tillner, H.-J. Lugauer  
Osram Opto Semiconductors GmbH  
Leibnizstr. 4, 93055 Regensburg, Germany

N. Tillner  
Institute of Semiconductor Technology  
Technische Universität Braunschweig  
Hans-Sommer-Straße 66, 38106 Braunschweig, Germany

P. Manley, C. Becker  
Nano-SIPPE  
Helmholtz-Zentrum Berlin für Materialien und Energie GmbH  
Albert-Einstein-Straße 16, 12489 Berlin, Germany

reproducible process for the deposition of high-quality AlN on sapphire is still a challenge.

A relatively new approach to decrease the TDD down to about  $5 \times 10^8 \text{ cm}^{-2}$  even for thin AlN layers below  $1 \mu\text{m}$  was introduced by Miyake et al.<sup>[12]</sup> This is also advantageous for the targeted UV-LED chip process, because a low AlN layer thickness results in a lower bow of the wafers. High-temperature annealing (HTA) at about  $1700^\circ\text{C}$  in  $\text{N}_2\text{-CO}$  atmosphere was applied for MOVPE-grown layers, leading to a rearrangement of the AlN crystal lattice, reducing the TDD by more than one order of magnitude. This promising approach can even be applied to epitaxially sputtered AlN,<sup>[13]</sup> which can help to avoid the sensitive nucleation process in MOVPE reactors. Face-to-face arrangement of the AlN/sapphire templates during HTA was also found to preserve the AlN surfaces from decomposition.<sup>[13]</sup> Therefore, the toxic  $\text{N}_2\text{-CO}$  ambient during annealing can be avoided. The HTA technique has greatly influenced the AlN/sapphire community in recent years. Even first UVC-LEDs have been successfully fabricated on HTA templates.<sup>[14]</sup> By adjusting the sputtering process, record values for low TDDs of  $2 \times 10^8 \text{ cm}^{-2}$  for AlN on sapphire were achieved.<sup>[15]</sup> Further analysis was conducted to gain a deeper understanding of the impact of HTA on the AlN material quality, for example, domain boundary movement,<sup>[16,17]</sup> extended AlON formation,<sup>[18]</sup> dislocation movement mechanisms via dislocation climbing,<sup>[19]</sup> and strain evolution.<sup>[20]</sup> The HTA process turned out to be a versatile process, which can also be applied to semipolar and nonpolar AlN on sapphire substrates<sup>[21,22]</sup> and to AlN layers on SiC substrates.<sup>[23]</sup>

However, a low TDD of the AlN is not the only issue to be solved along the path for realizing efficient UV-LEDs on AlN/sapphire templates. Due to internal total reflection at the planar AlN/sapphire interface, the major part of the generated light cannot be coupled out through the substrate. In this context, the AlN grown on nanoscale-patterned sapphire substrates (NPSSs) comes into focus. The nanosize pattern cannot only decrease the coalescence layer thickness compared with microsize patterns, but if arranged in a periodical way is also supposed to have a photonic crystal effect potentially avoiding parts of the internal total reflection.<sup>[24–26]</sup> Although the GaN growth on microsize-patterned sapphire substrates (PSS) is a state-of-the-art technology for blue LEDs, reports on UV-LEDs on NPSS are still limited.<sup>[27]</sup> Mainly due to the high sticking coefficient of Al, MOVPE growth of AlN on NPSS is challenging. Growth conditions have to be properly adjusted to suppress polycrystalline growth in the presence of non-c-plane-oriented sapphire facets.<sup>[28,29]</sup>

Our group has recently investigated the influence of an intermediate HTA step on the growth of planar AlN/sapphire templates.<sup>[30]</sup> We now extended this work to the investigation of AlN growth by MOVPE on NPSS with hole-type pattern. HTA of thin AlN seed layers is introduced to avoid layer cracking and to lower the TDD. Furthermore, a 265 nm UVC-LED on NPSS is demonstrated, and the influence of the patterned interface on the emission power is discussed.

## 2. Experimental Section

The c-plane-oriented sapphire substrates (2 in. diameter) with a nominal offcut of  $0.2^\circ$  toward the sapphire m-plane were

patterned by nanoimprint lithography (NIL). The patterning of nanoholes into sapphire was performed by inductively coupled plasma (ICP) etching in a SENTECH SI500 etcher. A multistep etching process using a hardmask was developed to protect on one hand the epi-ready sapphire surface between adjacent nanoholes against etching so that AlN growth can start on an undisturbed surface and on the other hand to realize steep nanohole sidewalls. In the first step, the NIL-resist mask was transferred into a  $\text{SiN}_x$  hardmask using a highly selective etching recipe based on fluorine chemistry. A short descum process was used to strip all resist residues prior to the sapphire etch step. The final sapphire surface after etching with a chlorine-based ICP process and a nitride removal process showed hexagonally arranged holes with a pitch of 600 nm, a hole diameter of 220 nm, and a depth of 200 nm (**Figure 1**). For comparison, AlN was grown in parallel on NPSS and on planar (nonpatterned) sapphire substrates in an  $11 \times 2$  in. MOVPE planetary reactor using the standard precursors trimethyl aluminum (TMAI) and ammonia ( $\text{NH}_3$ ). Hydrogen was used as the only carrier gas, and the total pressure was set to 50 mbar to avoid gas-phase prereactions. The process temperature ( $T_{\text{proc}}$ ) was measured pyrometrically from the backside of the heated substrate holders. Thus, the true temperature of the sample surface is expected to be about  $40^\circ\text{C}$  lower than  $T_{\text{proc}}$ . Prior to AlN deposition, the sapphire substrates were heated up to nucleation temperature of  $T_{\text{proc}} = 980^\circ\text{C}$ . At this temperature, a nucleation layer (NL) of 50 nm AlN was deposited at a rate of  $0.2 \mu\text{m h}^{-1}$  and an input group V to group III (V/III) ratio of 4000. Subsequently, 250 nm AlN was grown at a V/III ratio of 30, a growth rate of  $1.6 \mu\text{m h}^{-1}$ , and  $T_{\text{proc}}$  of  $1180^\circ\text{C}$ . During the MOVPE process, a LayTec EpiCurvIT<sup>®</sup> metrology system monitored the reflected light intensity at 405 nm wavelength from the front side of the wafer as well as the wafer curvature by three-beam laser deflection.

For HTA, MOVPE grown samples were transferred into a hot wall furnace. Annealing was done under  $\text{N}_2$  flow at a total pressure of 1000 mbar using the face-to-face configuration suggested by Miyake et al.<sup>[13]</sup> The oven was heated up with a temperature gradient of  $8^\circ\text{C min}^{-1}$  to  $1600^\circ\text{C}$  followed by a temperature gradient of  $4^\circ\text{C min}^{-1}$  to reach the targeted annealing temperatures ( $T_a$ ) of 1680 and  $1710^\circ\text{C}$ . These temperatures were kept constant

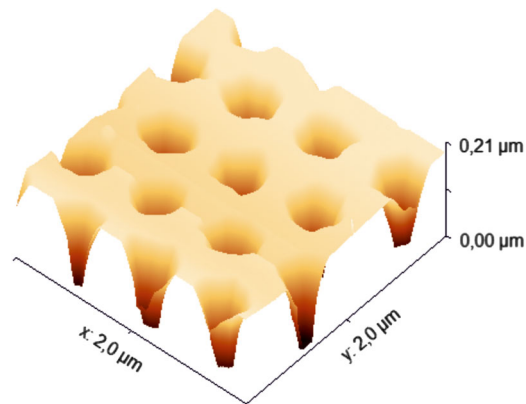


**Figure 1.** AFM image of the NPSS hole pattern with hexagonal arrangement and 600 nm pitch prepared by NIL.

for 1 h.  $T_a$  was measured with a type C thermocouple inside the oven 10 mm above the samples.

After the HTA treatment, the samples were placed back into the MOVPE reactor and overgrown with AlN at a relatively high temperature of  $T_{\text{proc}} = 1380^\circ\text{C}$ ,  $V/\text{III} = 840$ , and a growth rate of  $0.9\ \mu\text{m h}^{-1}$  to obtain a coalesced layer.

UV-LED heterostructures for emission at 265 nm were grown on the AlN/sapphire templates in a close coupled shower head MOVPE reactor starting with a 25 nm-thick layer graded from AlN to  $\text{Al}_{0.76}\text{Ga}_{0.24}\text{N}$ . This was followed by the n-side consisting of a 900 nm  $\text{Al}_{0.76}\text{Ga}_{0.24}\text{N}:\text{Si}$  current spreading layer, a 100 nm AlGa $\text{N}:\text{Si}$  transition layer, and a 200 nm  $\text{Al}_{0.65}\text{Ga}_{0.35}\text{N}:\text{Si}$  contact layer. The active region contains a threefold  $\text{Al}_{0.62}\text{Ga}_{0.38}\text{N}/\text{Al}_{0.48}\text{Ga}_{0.52}\text{N}$  multiquantum well (MQW) followed by a 10 nm-thick  $\text{Al}_{0.85}\text{Ga}_{0.15}\text{N}$  interlayer. The p-side consists of a 25 nm-thick  $\text{Al}_{0.75}\text{Ga}_{0.25}\text{N}:\text{Mg}$  electron blocking layer and a 200 nm-thick GaN:Mg contact layer.

Morphological properties were assessed by light microscopy and atomic force microscopy (AFM). The crystal properties were investigated by X-ray diffraction (XRD) measurements using a Philips X'Pert Pro system. Therefore, an XRD geometry with a fourfold 220 Ge monochromator and  $0.5\ \text{mm} \times 5\ \text{mm}$  aperture on the source side and a slit with an acceptance angle of  $1^\circ$  in front of the detector was used. Plan-view panchromatic cathodoluminescence (pan-CL) measurements were conducted at a temperature of 80 K and an acceleration voltage of 5 kV on AlGa $\text{N}$  MQW samples with a heterostructure identical to the one described previously but without the p-side. Electroluminescence (EL) measurements were conducted on wafer for the LED heterostructure using indium dots as contacts.

### 3. Results and Discussion

#### 3.1. AlN Growth Start on NPSS

For comparison, 300 nm AlN were grown simultaneously on NPSS and on planar sapphire substrates. In situ reflectometry and curvature measurements (Figure 2) show the same transients for the 405 nm reflectance during nucleation and heating up. The average reflectance value during the growth on NPSS after nucleation is slightly increasing indicating the desired smoothing of the sample surface (or increase in the c-planar portion of the surface) by lateral overgrowth. Although the curvature for the planar grown sample indicates almost no change in strain during growth, the AlN on NPSS grows with tensile strain. Because of the expected strain release of the AlN on NPSS due to lateral growth over the nanoholes, this behavior is rather counterintuitive.

To more closely investigate the differences in the growth start behavior, the surfaces of both 300 nm-thick AlN layers were imaged by AFM (Figure 3). The AlN layer on NPSS grows continuously, only interrupted by the holes predetermined by the NPSS (Figure 3a). In contrast, the layer on planar sapphire shows many small holes that can reduce strain much more effectively (Figure 3b) and hence are an explanation for lower tensile strain during growth. We assume that the difference in the AlN growth behavior on both kinds of substrates is caused by the influence of

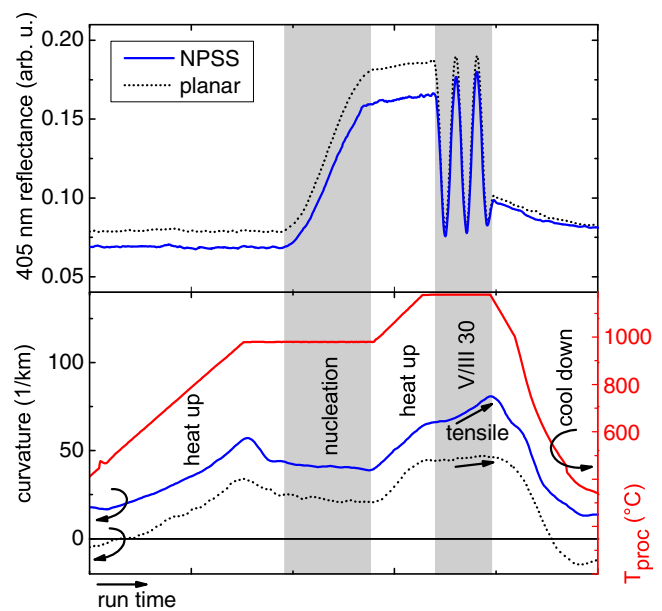


**Figure 2.** In situ measurement of the 405 nm reflectance from the sample surface, corresponding process temperature  $T_{\text{proc}}$  and curvature measurements during growth of 300 nm AlN on NPSS and planar sapphire. The curvature slope during the V/III 30 growth step shows higher tensile strain for AlN on NPSS than for AlN on planar sapphire.

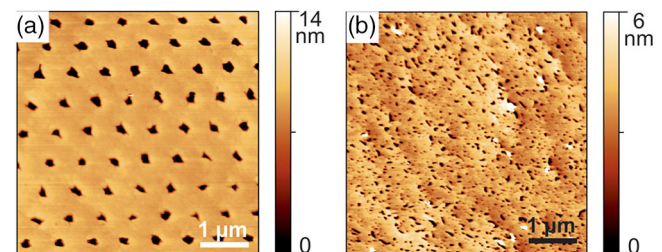


**Figure 3.** AFM surface topograms of 300 nm AlN on a) NPSS and b) planar sapphire grown simultaneously in the  $11 \times 2$  in. MOVPE reactor.

oxygen from the open sidewalls of the NPSS during growth start. Under  $\text{H}_2$  carrier gas, these sidewalls are not as stable as the c-plane sapphire surface<sup>[31]</sup> and therefore more oxygen is present during nucleation on NPSS compared with nucleation on planar sapphire. Oxygen in turn changes the nucleation conditions by shifting the mixed polarity growth start toward the Al-polar side.<sup>[32]</sup> With a lack of N-polar regions to be overgrown during the initial growth step, strain cannot be sufficiently reduced. After deposition of 300 nm AlN on NPSS, the layer is not yet coalesced but tensile strain brings it already close to cracking. One way to overcome this problem would be to optimize the growth start on NPSS, which could mean a time-consuming search for appropriate growth parameters and probably cannot be applied universally for hole patterns of different size and pitch. Another approach is to change the lattice constant of the 300 nm AlN starting layer to avoid tensile strain during further AlN growth.

### 3.2. HTA for Strain Management

Apart from improving the crystal quality, the method of HTA leads to an increase in compressive strain in AlN, which modifies the lattice constants toward smaller in-plane values.<sup>[13,30]</sup> Therefore, we applied HTA to the 300 nm starting layer on NPSS. We have chosen the starting layer thickness of 300 nm because at this layer thickness the AlN is not yet cracked but thick enough to prevent the destruction of the AlN/sapphire interface by AlON formation.<sup>[18]</sup> The samples were annealed at  $T_a$  of 1680 and 1710 °C. AFM topograms (Figure 4) show that the hole pattern is not affected by the annealing procedure. The AlN surface builds terraces that are smoother for the higher annealing temperature. XRD measurements of omega-rocking curves (XRC) of the 0002 reflection after annealing show a full width at half maximum (FWHM) of 100 and 90 arcsec for  $T_a$  of 1680 and 1710 °C, respectively. The XRC-FWHM of the 10–12 reflection is 410 arcsec for both samples. Therefore, both annealing temperatures lead to similar AlN crystal quality. The annealed samples were further overgrown together with a nonannealed sample for reference. MOVPE growth conditions were chosen, which use high temperature ( $T_{\text{proc}} = 1380$  °C) for lateral growth and high V/III ratio ( $V/III = 840$ ) to avoid build-up of surface steps by step bunching. Corresponding in situ reflectance and curvature measurements are shown in Figure 5. The medium value of the 405 nm reflectance during growth of 500 nm AlN stays constant at 0.14 and therefore indicates smooth surfaces on all samples. Curvature measurements reveal an increase in tensile strain for growth on the sample without HTA, whereas on both samples with HTA no further strain is observed. Although the layer on the nonannealed sample shows cracks particularly in the 1 cm edge region of the 2 in. wafer (Figure 6), no cracks were found on the two HTA samples. Therefore, HTA had been successfully applied for strain management during overgrowth on the hole pattern NPSS. AFM surface topograms of all overgrown samples prove that coalescence of the NPSS holes is already reached at a total AlN layer thickness of 800 nm. The surfaces look similar with terraces of about 700 nm width separated by steps of up to 2 nm height. The root-mean-square roughness for all topograms in Figure 7 is 0.6 nm. Only the step edges on the nonannealed sample most probably is caused by step pinning at dislocation sites.

The XRD measurements of 0002 and 10–12  $\omega$ -rocking curves were conducted to investigate the tilt and twist-related broadening of the reflections (Table 1). The XRCs on the sample without HTA were taken in a crack-free area and hence should not be

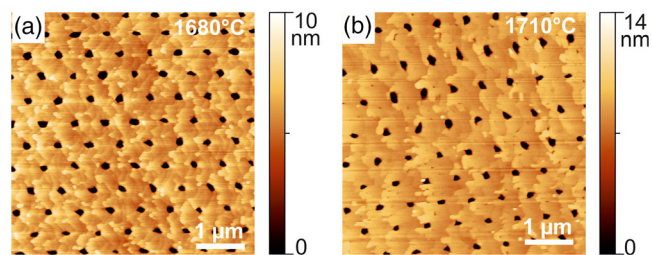


**Figure 4.** AFM surface topograms of 300 nm AlN after HTA for 1 h at a) 1680 °C and b) 1710 °C.

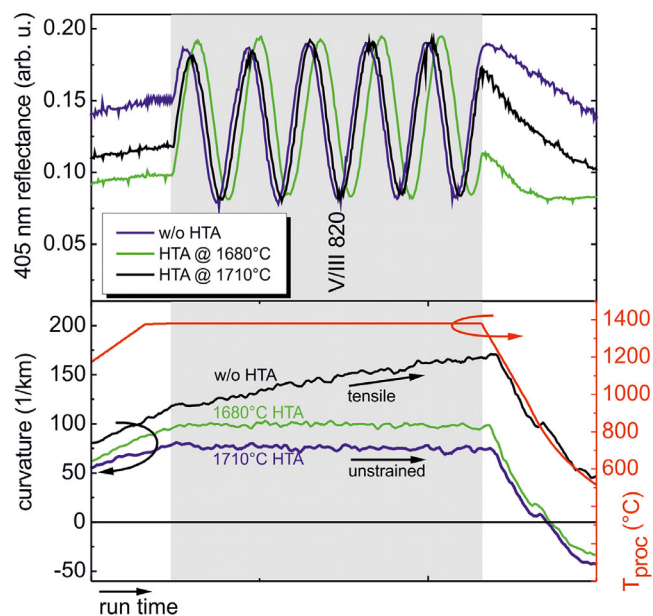


**Figure 5.** In situ measurement of the 405 nm reflectance from the sample surface and corresponding process temperature  $T_{\text{proc}}$  and curvature measurements during the growth of 500 nm AlN on NPSS with HTA at 1680 °C, at 1710 °C, and without intermediate HTA of the initial layer. The curvature slope during the V/III 820 growth step shows increasing tensile strain for nonannealed AlN on NPSS, whereas growth on annealed AlN on NPSS does not incorporate further strain.

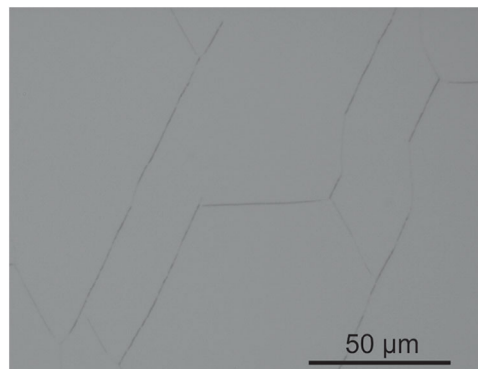


**Figure 6.** Light microscopy image of cracked 800 nm-thick AlN grown on NPSS without intermediate HTA step.

broadened by cracks. The results clearly show the beneficial effect of the intermediate HTA step for decreasing the 0002 XRC-FWHM from 300 to 90 arcsec and the 10–12 XRC-FWHM from 1650 to 430 arcsec, therefore decreasing the tilt and twist component, respectively. From XRC-FWHM measurements, TDDs were estimated<sup>[33,34]</sup> to be  $2 \times 10^9 \text{ cm}^{-2}$  for both samples with the intermediate HTA treatment in contrast to  $3.2 \times 10^{10} \text{ cm}^{-2}$  for the sample without HTA. The increase in the annealing temperature from 1680 to 1710 °C did not lead to further significant decrease in the TDD. Therefore, higher annealing temperatures, which can damage

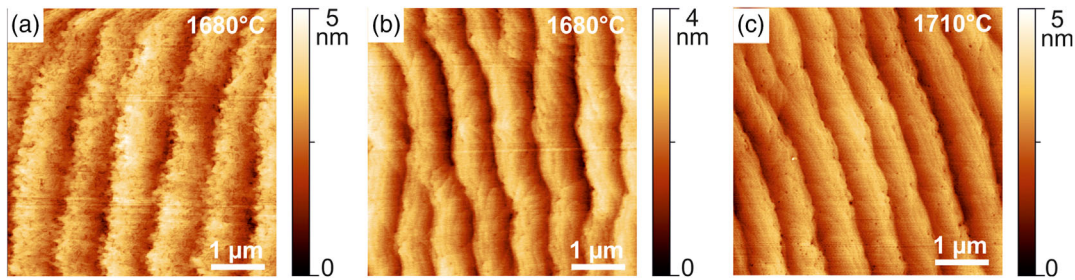


**Figure 7.** AFM surface topograms of coalesced 800 nm-thick AlN on NPSS a) without intermediate HTA step, and with initial 300 nm AlN layer annealed at b) 1680 °C and c) 1710 °C.

**Table 1.** XRC-FWHM of symmetric 0002 and skew-symmetric 10–12 reflection for 800 nm AlN grown on NPSS with and without intermediate HTA step. TDDs are calculated from the XRC-FWHM.

Sample	FWHM <sub>0002</sub> [arcsec]	FWHM <sub>10–12</sub> [arcsec]	TDD <sub>calc</sub> [ $\times 10^9 \text{ cm}^{-2}$ ]
w/o HTA	300	165	32
HTA@1680 °C	100	450	2
HTA@1710 °C	90	430	2

the AlN/sapphire interface by AlON formation,<sup>[18]</sup> do not give any benefit to the process. To summarize, with a calculated TDD of about  $2 \times 10^9 \text{ cm}^{-2}$  at an AlN layer thickness of only 800 nm plus the nanopattern at the AlN/sapphire interface, these templates are promising candidates to be used as a basis for UV-LEDs.

### 3.3. 265 nm UVC-LED on HTA AlN/NPSS

AlN/NPSS prepared with an intermediate HTA step at 1680 °C (HTA-AlN/NPSS) has been chosen for overgrowth with a UVC-LED heterostructure. In the same growth experiment an also high temperature annealed 740 nm-thick MOVPE AlN layer on planar sapphire (HTA-AlN/sapphire) was overgrown as reference. This planar AlN template had also been annealed at 1680 °C for 1 h, resulting in XRC-FWHMs of 70 and 520 arcsec for the 0002 and 10–12 reflection, respectively. Therefore, the calculated TDD of  $3 \times 10^9 \text{ cm}^{-2}$  is similar to that of the AlN/NPSS

template (Table 1). The pan-CL images of the MQW samples grown on both AlN templates (Figure 8) show centers of nonradiative recombination as dark spots. This dark spot density (DSD) was counted to be  $3 \times 10^9 \text{ cm}^{-2}$  for the planar template and  $2 \times 10^9 \text{ cm}^{-2}$  for the NPSS template, which is in good agreement with the calculated TDDs of the AlN templates. Thus, no further threading dislocations were introduced during the heterostructure growth. EL measurements on the full LED heterostructure show a single peak emission at 265 nm for both samples (Figure 9a). The light emission power–current  $L$ – $I$  curves (Figure 9b) show that the LEDs on both AlN templates have similar characteristics. Therefore, the HTA-AlN/NPSS template is a suitable substrate for UV-LEDs. NPSS has been reported to increase the LEE,<sup>[24–26]</sup> which was not observed here. To explain under which conditions the LEE can be increased wave optical simulations were performed. The transmittance through the AlN/sapphire interface the planar and patterned case using a simplified structure as shown in Figure 10a was calculated were absorption and reflection, especially of p-side and p-contact in the LED is represented by an omnidirectional mirror with reflectivity  $R$ . The nanostructured interface is modeled using the finite-element method. A plane wave source with 265 nm vacuum wavelength incident from the AlN is used. By varying the incident angle and polarization and obtaining the outgoing angles and polarizations of light, a scattering matrix could be constructed, which characterizes the interface. The reflection at the top interface of the AlN representing transmission and reflection from the LED structure was also characterized by a scattering matrix. This was obtained by assuming a mirror (Figure 10a) with an

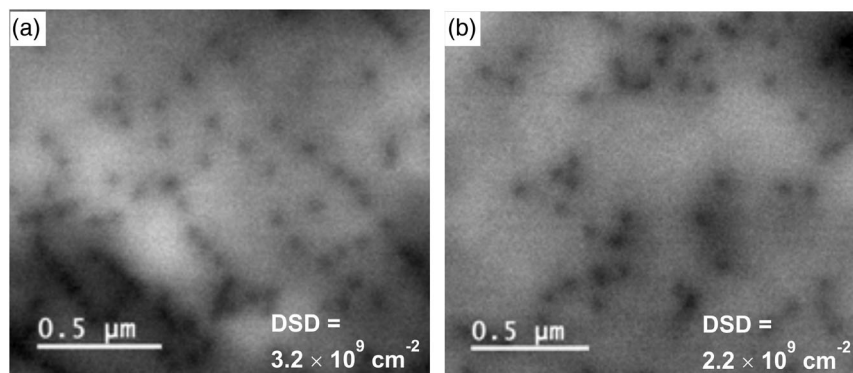


**Figure 8.** The pan-CL image of the UVC-LED heterostructure grown up to the MQW region on a) planar HTA-AlN/sapphire and b) HTA-AlN/NPSS.

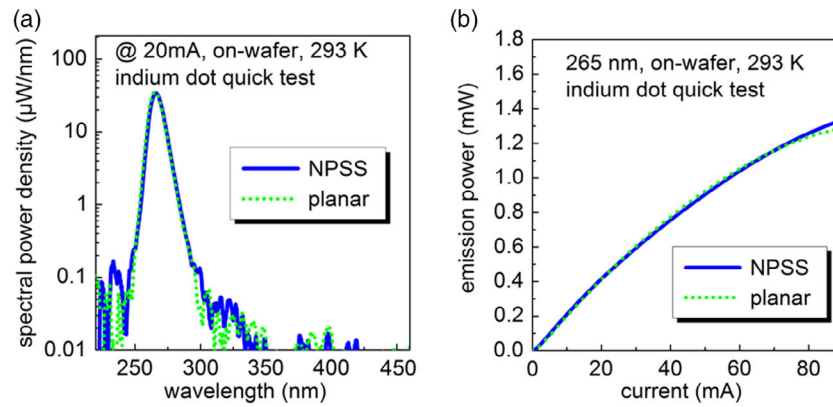


**Figure 9.** Emission spectra of UVC-LEDs grown on a) HTA-AlN/NPSS template and planar HTA-AlN/sapphire and b) corresponding  $L$ - $I$  characteristics measured on-wafer in bottom emission configuration.

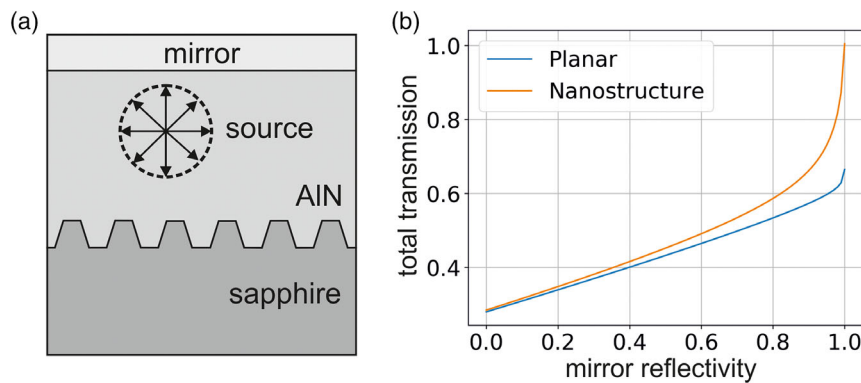


**Figure 10.** a) Schematic of the coupled system used for modeling the transmission of light emitted from AlN into sapphire. b) The total transmission for different values of reflectivity of the mirror shown in part (a) for the case of a planar AlN/sapphire interface and an AlN/NPSS interface with nanohole pattern.

angle-independent reflectivity which was varied from 0 to 1. Combining the two scattering matrices together, the propagation of light in the coupled system can be described. By assuming an isotropic emission of light inside the AlN layer, the total transmission from the AlN into the sapphire substrate could be obtained while considering multiple reflections at the nanostructured interface. The polarization of the light emitted inside the AlN was assumed to be equally weighted between TE and TM polarization. The results of the calculations (Figure 10b) suggest that in case of a low mirror reflectivity representing a heterostructure with absorbing p-side, the transmittance through the planar AlN/sapphire interface is similar to the transmittance through the nanopatterned interface. This leads to the conclusion that for an improvement of the light extraction efficiency due to an AlN/NPSS interface, the absorbing 200 nm-thick GaN:Mg p-side contact has to be replaced by a transparent p-side being capped with a highly reflective material.

#### 4. Conclusions

A 800 nm-thick, fully coalesced AlN was grown on 2 in. NPSS with hexagonally arranged holes and a pitch of 600 nm. By

applying HTA to a 300 nm-thick AlN starting layer on the NPSS, we successfully prevented the AlN film from cracking during further growth across the whole wafer, and at the same time the TDD was lowered by an order of magnitude from  $3.2 \times 10^{10}$  to  $2 \times 10^9 \text{ cm}^{-2}$ . We found that increasing the annealing temperature from 1680 to 1710 °C for the 1 h intermediate annealing step does not significantly improve the material quality so that a lower annealing temperature can be chosen to prevent damage of the AlN/sapphire interface during annealing. The usability of the 800 nm AlN/NPSS template for UVC-LEDs was proven by growth of a heterostructure emitting at 265 nm with single peak emission. No impact of the patterned AlN/sapphire interface on the light output power could be found compared with a heterostructure with planar AlN/sapphire interface. This is in good agreement with wave optical simulation results suggesting an improvement of the light transmittance through the AlN/sapphire interface only for a transparent p-side capped with a highly reflective material.

#### Acknowledgements

This work was partially funded by the German Federal Ministry of Education and Research (BMBF) within the Advanced UV for Life project

consortium (Grant Number: 03ZZ0134B) and by the German Research Foundation (DFG) within the Collaborative Research Center "Semiconductor Nanophotonics" (CRC 787) (Grant Number: 43659573). P.M. thanks the Helmholtz Association for funding within the Helmholtz Innovation Lab HySPRINT. Furthermore, the authors thank Torsten Petzke for technical assistance with the MOVPE machine.

## Conflict of Interest

The authors declare no conflict of interest.

## Keywords

AlN, high-temperature annealing, metalorganic vapor-phase epitaxy, nanopatterned sapphire substrates, ultraviolet light-emitting diodes

Received: September 21, 2019

Revised: December 1, 2019

Published online: January 27, 2020

- 
- [1] W. L. Morison, T. B. Fitzpatrick, *Phototherapy and Photochemotherapy of Skin Disease*, 2nd ed., Raven Press, New York **1991**.
- [2] M. Kneissl, J. Rass, *III-Nitride Ultraviolet Emitters*, Springer, Cham **2016**.
- [3] M. Würtele, T. Kolbe, M. Lipsz, A. Külberg, M. Weyers, M. Kneissl, M. Jekel, *Water Res.* **2011**, *45*, 1481.
- [4] H. Hirayama, T. Yatabe, N. Noguchi, N. Kamata, *Electron. Commun. Jpn.* **2010**, *93*, 24.
- [5] N. Okada, N. Kato, S. Sato, T. Sumii, T. Nagai, N. Fujimoto, M. Imura, K. Balakrishnan, M. Iwaya, S. Kamiyama, H. Amano, I. Akasaki, H. Maruyama, T. Takagi, T. Noro, A. Bandoh, *J. Cryst. Growth* **2007**, *298*, 349.
- [6] H. Hirayama, S. Fujikawa, N. Noguchi, J. Norimatsu, T. Takano, K. Tsubaki, N. Kamata, *Phys. Status Solidi A* **2009**, *206*, 1176.
- [7] H. Hirayama, S. Fujikawa, J. Norimatsu, T. Takano, K. Tsubaki, N. Kamata, *Phys. Status Solidi C* **2009**, *6*, S356.
- [8] V. Kueller, A. Knauer, U. Zeimer, H. Rodriguez, A. Mogilatenko, M. Kneissl, M. Weyers, *Phys. Status Solidi C* **2011**, *8*, 2022.
- [9] GenUV, [http://www.geni-uv.com/ain\\_template.php](http://www.geni-uv.com/ain_template.php) (accessed: July 2019).
- [10] MSESUPPLIES, <https://www.msesupplies.com/products/2-inch-aluminum-nitride-aln-template-on-sapphire-0001-aln?variant=22039235716> (accessed: July 2019).
- [11] Nitride Solutions, <http://nitridesolutions.com/products/> (accessed: July 2019).
- [12] H. Miyake, G. Nishio, S. Suzuki, K. Hiramatsu, H. Fukuyama, J. Kaur, N. Kuwano, *Appl. Phys. Express* **2016**, *9*, 025501.
- [13] H. Miyake, C.-H. Lin, K. Tokoro, K. Hiramatsu, *J. Cryst. Growth* **2016**, *456*, 155.
- [14] N. Susilo, S. Hagedorn, D. Jaeger, H. Miyake, U. Zeimer, C. Reich, B. Neuschulz, L. Sulmoni, M. Guttman, F. Mehnke, C. Kuhn, T. Wernicke, M. Weyers, M. Kneissl, *Appl. Phys. Lett.* **2018**, *112*, 041110.
- [15] K. Uesugi, Y. Hayashi, K. Shojiki, H. Miyake, *Appl. Phys. Express* **2019**, *12*, 065501.
- [16] J. Kaur, N. Kuwano, K. Jamaludin, M. Mitsuahara, H. Saito, S. Suzuki Satoshi Hata, H. Miyake, K. Hiramatsu, H. Fukuyama, *Appl. Phys. Express* **2016**, *9*, 065502.
- [17] S. Xiao, R. Suzuki, H. Miyake, S. Harada, T. Ujihara, *J. Cryst. Growth* **2018**, *502*, 41.
- [18] S. Hagedorn, S. Walde, A. Mogilatenko, M. Weyers, L. Cancellara, M. Albrecht, D. Jaeger, *J. Cryst. Growth* **2019**, *512*, 142.
- [19] L. Cancellara, S. Hagedorn, S. Walde, D. Jaeger, S. Washiyama, I. Gamov, K. Irmscher, T. Markurt, R. Collazo, Z. Sitar, M. Weyers, M. Albrecht, presented at IWN, Kanazawa, Japan, November, 2018.
- [20] M. X. Wang, F. J. Xu, N. Xie, Y. H. Sun, B. Y. Liu, W. G. Ge, X. N. Kang, Z. X. Qin, X. L. Yang, X. Q. Wang, B. Shen, *Appl. Phys. Lett.* **2019**, *114*, 112105.
- [21] M. Jo, N. Morishita, N. Okada, Y. Itokazu, N. Kamata, K. Tadatomo, H. Hirayama, *AIP Adv.* **2018**, *8*, 105312.
- [22] D. V. Dinh, N. Hu, Y. Honda, H. Amano, M. Pristovsek, *J. Cryst. Growth* **2018**, *498*, 377.
- [23] K. Uesugi, Y. Hayashi, K. Shojiki, S. Xiao, K. Nagamatsu, H. Yoshida, H. Miyake, *J. Cryst. Growth* **2019**, *510*, 13.
- [24] E. Matioli, C. Weisbuch, *J. Phys. D: Appl. Phys.* **2010**, *43*, 354005.
- [25] D. Lee, J. Lee, J. Jang, I.-S. Shin, L. Jin, J. H. Park, J. Kim, J. Lee, H.-S. Noh, Y.-I. Kim, Y. Park, G.-D. Lee, Y. Park, J. Kim, E. Yoon, *Appl. Phys. Lett.* **2017**, *110*, 191103.
- [26] Y. K. Ooi, J. Zhang, *IEEE Photonics J.* **2018**, *10*, 8200913.
- [27] P. Dong, J. Yan, J. Wang, Y. Zhang, C. Geng, T. Wei, P. Cong, Y. Zhang, J. Zeng, Y. Tian, L. Sun, Q. Yan, J. Li, S. Fan, Z. Qin, *Appl. Phys. Lett.* **2013**, *102*, 241113.
- [28] S. Hagedorn, A. Knauer, A. Mogilatenko, E. Richter, M. Weyers, *Phys. Status Solidi A* **2016**, *213*, 3178.
- [29] L. Zhang, F. Xu, J. Wang, C. He, W. Guo, M. Wang, B. Sheng, L. Lu, Z. Qin, X. Wang, B. Shen, *Sci. Rep.* **2016**, *6*, 35934.
- [30] S. Walde, S. Hagedorn, M. Weyers, *Jpn. J. Appl. Phys.* **2019**, *58*, SC1002.
- [31] Y. Kumagai, T. Igi, M. Ishizuki, R. Togashi, H. Murakami, K. Takada, A. Koukitu, *J. Cryst. Growth* **2012**, *350*, 60.
- [32] S. Mohn, N. Stolyarchuk, T. Markurt, R. Kirste, M. P. Hoffmann, R. Collazo, A. Courville, R. Di Felice, Z. Sitar, P. Vennéguès, M. Albrecht, *Phys. Rev. Appl.* **2016**, *5*, 054004.
- [33] P. Gay, P. B. Hirsch, A. Kelly, *Acta Metall.* **1953**, *1*, 315.
- [34] S. R. Lee, A. M. West, A. A. Allerman, K. E. Waldrip, D. M. Follstaedt, P. P. Provencio, D. D. Koleske, C. R. Abernathy, *Appl. Phys. Lett.* **2005**, *86*, 241904.